Combustion and Flame 159 (2012) 1840–1850

Contents lists available at SciVerse ScienceDirect

Combustion and Flame

journal homepage: www.elsevier.com/locate/combustflame

Structure of atmospheric-pressure fuel-rich premixed ethylene flame with and without ethanol

Ilya E. Gerasimov [a,b], Denis A. Knyazkov [a,*], Sergey A. Yakimov [a], Tatyana A. Bolshova [a], Andrey G. Shmakov [a], Oleg P. Korobeinichev [a]

[a] Institute of Chemical Kinetics and Combustion, Novosibirsk 630090, Russia
[b] Novosibirsk State University, Novosibirsk 630090, Russia

ARTICLE INFO

Article history:
Received 9 April 2011
Received in revised form 20 September 2011
Accepted 22 December 2011
Available online 23 January 2012

Keywords:
Ethylene
Ethanol
Flame structure
Combustion intermediates
Molecular beam mass-spectrometry

ABSTRACT

Effect of ethanol (EtOH) addition to unburnt gas mixture on the species pool in a fuel-rich flat, premixed, laminar ethylene flame at atmospheric pressure is studied experimentally and by chemical kinetic modeling. Mole fraction profiles as a function of height above burner of various stable and labile species including reactants, major products and intermediates (C_1–C_4 hydrocarbons) are measured using molecular beam mass spectrometry with electron ionization in $C_2H_4/O_2/Ar$ and $C_2H_4/EtOH/O_2/Ar$ flames. The experimental profiles are compared with those calculated using three different chemical kinetic mechanisms. Performances and deficiencies of the mechanisms are discussed. An analysis of the mechanisms is carried out in order to identify the reason of the ethanol effect on the mole fraction of propargyl, the main precursor of benzene. A modification of some mechanisms in order to improve their capability to predict acetylene and diacetylene mole fraction profiles is proposed.

1. Introduction

Recent extensive studies of the combustion chemistry of oxygenates have been motivated by the ability of these compounds to decrease concentrations of various toxic species such as CO, NO_x, and soot in combustion products. This is of great practical significance not only for environmental protection, but also for promoting combustion in internal combustion engines, gas turbines, furnaces, and other combustion devices. The study of the combustion mechanism of oxygenates and their blends with hydrocarbons is of particular importance for the development of novel biofuels and their blends with conventional fossil fuels to meet the needs of the transport and power industries. A comprehensive survey of investigations of combustion chemistry for various oxygenated fuels can be found elsewhere [1].

One of the most promising oxygenates for practical use is ethanol, which is currently produced on an industrial scale from biomass. Using blends of petroleum-based fuels with biofuels, such as ethanol, is commonly suggested with the aim to reduce carbon dioxide emission from combustion of fossil fuels. However, when ethanol is added to conventional fuels, an increase in concentrations of carbonyl compounds in combustion products occurs under certain conditions [2]. Therefore, the combustion chemistry of ethanol and its blends with other hydrocarbons is of particular interest. Experimental data on spatial variations in concentrations of various species in flames are a major source of information on the chemistry and chemical kinetic mechanism of combustion for a particular fuel. For this reason, considerable effort has been made to elucidate the structure of premixed and diffusion flames of ethanol [3–6] and its blends [7–16] with various hydrocarbons.

Kohse-Höinghaus et al. [3] and Vandooren et al. [4,5] studied the structure of premixed ethanol/oxygen/argon flames stabilized on a flat burner at 50 mbar using electron-ionization molecular beam mass spectrometry (EI-MBMS). Saxena and Williams [6] measured spatial variations in concentrations of reactants, final products, and some stable intermediates in partially premixed and nonpremixed counterflow $C_2H_5OH/O_2/N_2$ flames at atmospheric pressure using microprobe sampling and chromatography.

The effect of the addition of ethanol on the combustion of various hydrocarbons has been investigated by measuring concentrations of various species in premixed flames of ethylene [7,8], propylene [9,16], heptane [10,11], gasoline [12], and in diffusion ethylene flames [13–15] with the addition of ethanol. Ethylene is an important intermediate product formed in large amounts during oxidation of heavy hydrocarbons. Thus, ethylene flame can be used as a simplified model to study the combustion of conventional hydrocarbon fuels. It is suggested that the trends revealed in the analysis of the effect of ethanol addition on ethylene

* Corresponding author. Address: Institute of Chemical Kinetics and Combustion, Institutskaya St. 3, Novosibirsk 630090, Russia. Fax: +7 383 330 73 50.
E-mail address: knyazkov@kinetics.nsc.ru (D.A. Knyazkov).

0010-2180/$ - see front matter © 2012 The Combustion Institute. Published by Elsevier Inc. All rights reserved.
doi:10.1016/j.combustflame.2011.12.022

combustion will be true for other hydrocarbon fuels. In the above-mentioned studies of ethylene/ethanol systems [7,8,13–15], emphasis was primarily on the effect of ethanol on the formation of soot and polyaromatic hydrocarbons (PAHs) that are soot precursors.

In our earlier work [7], we discussed a contribution of recent studies [8,13–15] to the understanding of ethanol effect on ethylene flames. Previously [7] we investigated the effect of ethanol addition on the formation of precursors of PAHs and soot in low-pressure (30 torr) premixed rich ethylene flames by studying the structure of ethylene flames with and without ethanol using molecular beam mass spectrometry with synchrotron VUV radiation and computer modeling based on a detailed kinetic mechanism. The mechanism was created by combining two mechanisms from the literature: the mechanism of Frenklach and coworkers [17,18] for ethylene combustion and the ethanol oxidation mechanism proposed by Marinov [19]. The model was shown to qualitatively describe the structure of the flames and correctly predict general trends in the effect of ethanol addition on the mole fractions of intermediate products in the flame. The mole fraction of benzene and propargyl radicals, the main PAH precursors, was found to be lower in the flame with ethanol than in the pure ethylene flame. Analysis of the main reaction pathways for benzene formation in the flames with and without ethanol has shown that when part of ethylene in the initial combustible mixture is replaced with ethanol, the fraction of carbon forming soot precursors decreases due to the existence of ethanol reaction pathways producing species that later do not yield PAHs and soot precursors. This conclusion is in agreement with those made by Wu and coworkers [8].

This paper reports an extension of our previous work [7] to the case of atmospheric pressure. Our goal was to study how the replacement of part of ethylene with ethanol in an atmospheric-pressure premixed fuel-rich ethylene/oxygen/argon flame would influence the species pool in the flame. Due to the current interest in the problem of soot reduction in combustion products, in the present study, as in [7], we used fuel excess conditions and paid particular attention to species that could be involved in the formation of soot precursors. Using EI-MBMS and numerical modeling, we studied and compared the structure of two flat flames with the same equivalence ratio $\varphi = 1.7$: a pure ethylene flame and a flame in which ethylene was partially replaced with ethanol. The experimental results were compared with numerical results obtained using three different detailed chemical kinetic mechanisms.

2. Experimental procedure

The flames were stabilized on a Botha–Spalding flat burner at atmospheric pressure. The burner consisted of a perforated brass disk 16 mm in diameter and 3 mm thick (diameter of holes 0.5 mm, hole separation 0.7 mm) placed in a brass housing with a cooling jacket. The burner was filled with 3 mm diameter stainless steel balls to uniform flow speed at the burner surface and to thoroughly heat the flow. The effective burner diameter was 16 mm, the same as that of the perforated disk. The cooling jacket was thermostated by water at 90 °C. Inlet gas fluxes were set by mass flow controllers (MKS Instruments Inc.). The ethanol flux was introduced into the fresh mixture by passing of a flow of argon through an EtOH-filled bubbler thermostated at 40 °C. In the present work, two flames with the same equivalence ratio ($\varphi = 1.7$) were studied: an ethylene flame ($C_2H_4/O_2/Ar = 0.088/0.155/0.757$) and a flame with a 1:1 ratio of ethylene to ethanol ($C_2H_4/C_2H_5OH/O_2/Ar = 0.044/0.044/0.155/0.757$). In both flames, the flow rate of the cold mixture, temperature of which was 293 K, was maintained at 25.8 cm^3/s.

Species mole fractions in the flame as a function of height above the burner (HAB) were measured using the MBMS setup in Novosibirsk, which is detailed in [20,21] and has been used previously to measure atmospheric-pressure flame structures, see, e.g., [22,23]. The flame-burning area was sampled by a thin-walled quartz cone nozzle with a 40° inner angle, a 0.08 mm orifice diameter, and 0.08 mm wall thickness at the probe tip. The central part of the supersonic jet was extracted by a stainless steel skimmer and ionized in the ionization source of the mass spectrometer. The MBMS setup was equipped with a MS-7302 quadrupole mass-spectrometer with soft electron-impact ionization (spread in ionization energies of ±0.25 eV, this corresponds to basis width of the electron energy distribution function). Electron energies were selected for each species analyzed in order to obtain a signal-to-noise ratio high enough, without interferences from fragmentation of other species. Energies of ionizing electrons for most of the species were the same or close to those used by Bhargava and Westmoreland in [24], who studied the structure of rich ethylene/oxygen/argon flames stabilized on a flat burner at 20 torr. The signal intensity at $m/z = 39$ (propargyl radical) was measured at higher electron energy than that used in [24] (see Table 1). More details are given in Section 4.

Mole fraction profiles were derived from intensity profiles using the following procedure. All intensity profiles were normalized to the argon profile to eliminate the dependence on the temperature of the sample. Reactants (C_2H_4, C_2H_5OH, O_2) were calibrated to match the initial cold-flow mole fractions. Mole fractions of the intermediate species were evaluated using a technique similar to those used in our previous work [7] and by other authors [25]. Ion signal intensity (I_i) is related to the mole fraction of species i (X_i) at temperature T and the setup sensitivity to this species (S_i) by the simple relation

$$I_i = S_i(T)X_i, \tag{1}$$

The sensitivity S_i can be represented as

$$S_i(T) = A\sigma_i(E)D(m)F(T,P)N, \tag{2}$$

where A is a constant of proportionality; σ_i (E) is the ionization cross-section for species i at electron energy E; $D(m)$ is the mass discrimination factor [26–28]; $F(T,P)$ is an empirical function that relates the molecular beam density to the flame pressure P and local temperature T, N is the flux of ionizing electrons. The function $F(T,P)$ is determined by the geometric and gas-dynamic characteristics of the sampling cone and skimmer and is the same for all species in the probe. Eqs. (1) and (2) for species i and j lead to the following relation:

$$I_i/I_j = [\sigma_i(E_i)/\sigma_j(E_j)][D(m_i)/D(m_j)][X_i/X_j], \tag{3}$$

Mole fraction of species i can be evaluated if the ion signals of species i and j and the mole fraction of species j are known. Here, species j is considered as a reference species with known mole fraction, which is determined through direct calibration (reactants) or C-, O- element balance (CO_2, H_2O). Ionization cross sections for most of the species were taken from the NIST Electron Impact Cross Section Database [29]. For species for which data were not available in the NIST database, ionization cross sections were taken from [30] or estimated by the method described in [31]. Mass discrimination factors were determined experimentally using a number of multicomponent mixtures of known composition consisting of gases with different molecular weights (the main component of the mixtures was argon). These mixtures were preliminary heated to 473 K to prevent clustering of argon in the molecular beam. These experiments showed that the $D(m_i)/D(m_j)$ ratio was very close to unity under our experimental conditions.

The ratio of CO and CO_2 mole fractions in the post-flame zone was evaluated by Eq. (3). The individual mole fractions of CO and

Table 1
Species measured in the pure ethanol flame and in the ethylene/ethanol flame. IE: ionization energy (from [39]); $\sigma(E)$: electron ionization cross section (literature references are given); RICS (relative ionization cross section): calibration using Eq. (3).

m/z	Species	Species name	IE (eV)	σ (E)	Energy of ionizing electrons (eV)		Calibration method, comments
					Westmoreland [24]	Used in this work	
2	H_2	Hydrogen	15.43	[29]	17.2	18.0	RICS vs H_2O
16	CH_4	Methane	12.71	[29]	14.5	15.0	RICS vs H_2O
18	H_2O	Water	12.62	[29]	15.05	15.0	O-element balance
26	C_2H_2	Acetylene	11.41	[29]	12.4	12.4	RICS vs C_2H_4
28	C_2H_4	Ethylene	10.53	[29]	12.2	13.0	Direct
28	CO	Carbon monoxide	14.01	[29]	16.5	15.0	C-element balance
30	CH_2O	Formaldehyde	10.88	[29]	12.85	13.0	RICS vs O_2, not separated
30	C_2H_6	Ethane	11.55	[29]	–		
32	O_2	Oxygen	12.07	[29]	14.5	16.5	Direct
39	C_3H_3	Propargyl radical	8.68	[29]	9.9	12.0	RICS vs O_2
40	C_3H_4	Allene	10.22	[29]	11.4	13.0	RICS vs O_2, not separated
40	C_3H_4	Propyne	10.48	[29]			
40	Ar	Argon	15.76	-	18.0	16.3	-
42	C_3H_6	Propene	9.74	[29]	11.4	12.0	RICS vs O_2, not separated
42	CH_2CO	Ketene	9.6	[31]	–		
44	CH_3CHO	Acetaldehyde	10.22	[31]	11.4	12.0	RICS vs C_2H_5OH
44	CO_2	Carbon dioxide	13.80	[29]	16.0	16.0	C-element balance
46	C_2H_5OH	Ethanol	10.5	[30]	–	16.0	Direct
50	C_4H_2	Diacetylene	10.18	[29]	11.25	12.0	RICS vs CO_2
54	C_4H_6	1,3-Butadiene	9.23	[29]	11.25		Direct

CO_2 in the post-flame zone were calculated by C atom balance and were then used to determine mole fraction profiles of these species. The H_2O mole fraction in the post-flame zone and H_2O mole fraction profile were obtained by O atom balance. Mole fractions of other species were evaluated using Eq. (3). The mole fraction uncertainty for the flame reactants and major products (C_2H_4, C_2H_5OH, O_2, CO, CO_2, H_2O) was estimated to be ±15% of the maximum mole fraction values. For other species, mole fractions were determined to within a factor of about 2.

The uncertainties indicated above are mainly due to calibration errors. The effect of ethanol on the species mole fraction profiles (that is the change in a mass peak intensity signal when the fuel is changed from pure ethylene to ethylene/ethanol mixture) is determined within the accuracy of measurement of mass peak intensity. The measurement errors of mass peak intensities are mainly statistical and are reduced in the experiments to minimum by increasing (within reasonable limits) the measurement time and the number of measurements of signal intensity for every mass peak. The resulting uncertainty in determination of mass peak signal intensity depends on many factors (background signal, species mole fraction in the flame, setup sensitivity to a particular species, etc.) and is different for various mass peaks, but for most species, which we measured, this uncertainty is not higher than 10%.

Flames temperature profiles were measured by a Pt/Pt+10%Rh thermocouple welded from wire 0.02 mm in diameter, covered with a thin layer of SiO_2 to prevent catalytic recombination of radicals on the thermocouple surface. The resulting thermocouple had a diameter of 0.05 mm and a shoulder length of about 3 mm, providing negligible heat losses to the cold ends. The construction of the mounting unit for the thermocouple was described earlier [20]. A correction for radiation heat loss was applied as described elsewhere [32,33]. The temperature was measured with an accuracy of ±25 K.

The sampling probe inevitably induces gas-dynamic and thermal perturbations in the flame. This probe effect was taken into account as described in [23]. Gas-dynamic perturbations were accounted for by shifting the mole fraction profiles upstream by the distance $\Delta Z \sim d\sqrt{\frac{Q}{SV}}$, where d is the diameter of the probe orifice, Q is the volumetric flow rate through the orifice, S is the area of the orifice, and V is the linear velocity of the flow riding onto the probe [34]. The maximum shift corresponds to the position of the probe near the burner and comprises about 0.5 mm ($Q = 0.98$ cm^3/s, $V = 16$ cm/s, $S = 5.54 \times 10^{-5}$ cm^2, $d = 0.08$ mm). For consideration of thermal perturbations, temperature profiles were measured using the thermocouple positioned at 0.2 mm from the tip of the probe. These temperature profiles were used as input data for computer simulation of the flame structure.

3. Modeling

Numerical modeling was performed using the PREMIX code from the CHEMKIN II package. Three different detailed chemical kinetic mechanisms were employed.

The first chemical kinetic mechanism (mechanism 1) was similar to that used in [35] and in our previous work [7]. It consisted of two parts: the base mechanism for hydrocarbon oxidation developed by Frenklach and co-workers [17,18] and the ethanol oxidation mechanism taken from Marinov [19]. The base mechanism (Frenklach's) includes pyrolysis and oxidation of C_1 and C_2 species, formation of heavy linear hydrocarbons up to C_6 species, formation of benzene and further reactions leading to pyrene, and oxidation pathways of aromatic species. There are three versions of this mechanism available: for 90 torr, 1 bar, and 10 bar. In the present kinetic study, we used the second version. However, this mechanism does not include ethanol and the products and reactions of its transformation, so they were taken from Marinov's mechanism. The reactions selected from the ethanol mechanism were the initial reactions of the molecules themselves such as hydrogen abstraction and unimolecular decomposition, along with reactions of the resulting products that eventually produced species present in the base mechanism. The thermodynamic data were also combined to provide the required input data. The resultant mechanism contained 121 species and 708 reactions, of which 20 species and 164 reactions were added from the ethanol mechanism. This kinetic mechanism together with thermochemistry and transport data files in Chemkin format is given in Supplemental material (mmc1). To ensure that the combined mechanism had the same predicting ability for the pure ethylene flame as the base mechanism, we simulated the ethylene flame structure using both mechanism 1 and Frenklach's mechanism. As a result, complete

agreement was obtained between mole fraction profiles of various species obtained with these mechanisms. We also tested mechanism 1 and the original Marinov's mechanism against earlier experimental data obtained by Leplat et al. [5] for the structure of a low pressure ethanol flame. The following results were obtained: (a) Marinov's mechanism reproduces quite satisfactorily the experimental results, (b) mechanism 1 gives very close mole fraction profiles to those obtained with the original Marinov's model (the differences between the calculated profiles using different models are much less than the errors of the experiments). Furthermore, we simulated, using these mechanisms, the structure of a premixed atmospheric pressure ethanol flame (C_2H_5OH/O_2/Ar = 0.088/0.155/0.757, other flame conditions were the same as described in Section 2) and also observed mole fraction profiles, obtained with these mechanisms, to be in close agreement.

The second mechanism (mechanism 2) was combined similarly to the first one with the only difference that the USC-Mech-II mechanism developed by Wang et al. [36] was used as the base mechanism. The resultant mechanism contained 116 species and 823 reactions, of which 5 species and 39 reactions were taken from Marinov's mechanism for ethanol oxidation. This kinetic mechanism together with thermochemistry and transport data files in Chemkin format is given in Supplemental material (mmc2). Mechanism 2 was found to give the same mole fraction profiles in the pure ethylene flame as the base USC-Mech-II mechanism.

The third mechanism (mechanism 3) was the one proposed by Konnov for combustion of small hydrocarbons [37]. This mechanism involves the reactions of ethanol, so that it was used as released by the developer (without any modifications). It consists of 1208 reactions involving 127 species.

To analyze the reaction pathways in flames, we investigated C-element fluxes from species to species using the Kinalc code [38], a post-processor of Premix output files.

4. Results and discussion

Table 1 shows the species measured in the flames studied: reactants (C_2H_4, O_2, C_2H_5OH), major stable products (CO, CO_2, H_2, H_2O), and intermediate species (C_1–C_4 hydrocarbons). Also shown in this table are their ionization energies, literature data on ionization cross-sections, energies of ionizing electrons (used in this work and those used by Bhargava and Westmoreland [24] for comparison), and the calibration method used. The set of species that we expected to detect in the flames was determined from the results of previous numerical simulations using mechanism 1. We selected species that, according to the simulation data, have relatively high mole fractions (not lower than 10 ppm). Unfortunately, we were unable to measure with reasonable accuracy the signal intensities at $m/z = 15$ (CH_3), 17 (OH), 27(C_2H_3), 41 (C_3H_5), 52 (C_4H_4), 77(C_6H_5), and 78 (C_6H_6), despite the fact that to measure them, we used energies of ionizing electrons even higher than those used by Bhargava and Westmoreland [24]. Some of these species (CH_3, C_3H_5, C_4H_4, C_6H_6) were, however, measured successfully in low pressure conditions [7]. We suppose that in the case of atmospheric pressure conditions the reasons of the failure of the species measurement could be as following: first, low signal to noise ratio due to a high background signal at the corresponding m/z ratios, and, second, the actual concentrations of these species are indeed lower than the detection limit. Some masses correspond to species that had very close ionization energies, in particular, $m/z = 30$ (formaldehyde CH_2O and ethane C_2H_6), 40 (allene and propyne having a common formula C_3H_4), and 42 (propene C_3H_6 and ketene CH_2CO). In our previous study [7], synchrotron VUV radiation with high energy resolution was used for ionization, so we could separate these species, however in this work we were unable to identify these compounds separately due to fairly wide spread (specified above) in electron energies. Experimental temperature and mole fraction profiles for all detected species together with mole fraction profiles calculated using mechanisms 1, 2, and 3 in both pure ethylene and ethylene/ethanol flames are given in the tables in Supplementary material (mmc3).

4.1. Temperature and major species

Temperature profiles of the flames measured near the sampling probe at 0.2 mm from its tip are presented in Fig. 1. As can be seen from the figure, replacing 50% of ethylene with ethanol does not result in a significant change in the temperature distribution. The width of the flame zone remains much the same, about 1 mm. The post-flame temperature in the ethylene flame us 1680 K, and in the flame with ethanol, it is only 20 K higher. However, this change is less than the uncertainty of the thermocouple measurements. The fact that the temperature distribution in both flames is practically the same facilitates comparison of mole fraction profiles of species and hence the reaction kinetics in these flames because in considering the processes in the flames at the same height above the burner, one can neglect the temperature effect.

Measured and simulated mole fraction profiles of reactants (C_2H_4, O_2, C_2H_5OH) and major products (CO, CO_2, H_2, H_2O) in both flames (with and without ethanol) are shown in Fig. 2. Because the calculations with the three chemical kinetic mechanisms give similar mole fraction profiles for these species, Fig. 2 shows only the profiles calculated with mechanism 1. As seen from Fig. 2, the experimental and modeling results indicate that replacing 50% of ethylene with ethanol in the fresh mixture leads to a change in the composition of the final products, i.e., to an increase in the mole fractions of CO_2, H_2O, and H_2 and a decrease in the CO mole fraction. The width of the flame zone, however, does not change (this is also evident from the temperature profiles in Fig. 1). One can conclude that reaction mechanism 1 (and other mechanisms) well reproduces the mole fraction profiles of reactants, as well as H_2 and CO_2 in these flames. Some disagreement can be observed only for water and carbon monoxide, but it is within the measurement error. In both flames, the mole fractions of CO measured in the post-flame zone are about 15% higher than the calculated values. This is almost beyond the measurement error and can be explained by the fact that in the determination of the carbon

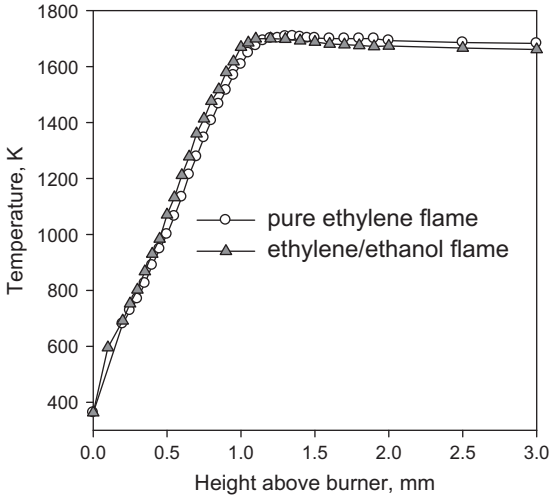

Fig. 1. Temperature profiles measured by the thermocouple positioned at 0.2 mm from the tip of the sampling probe in pure ethylene flame and in the ethylene/ethanol flame.

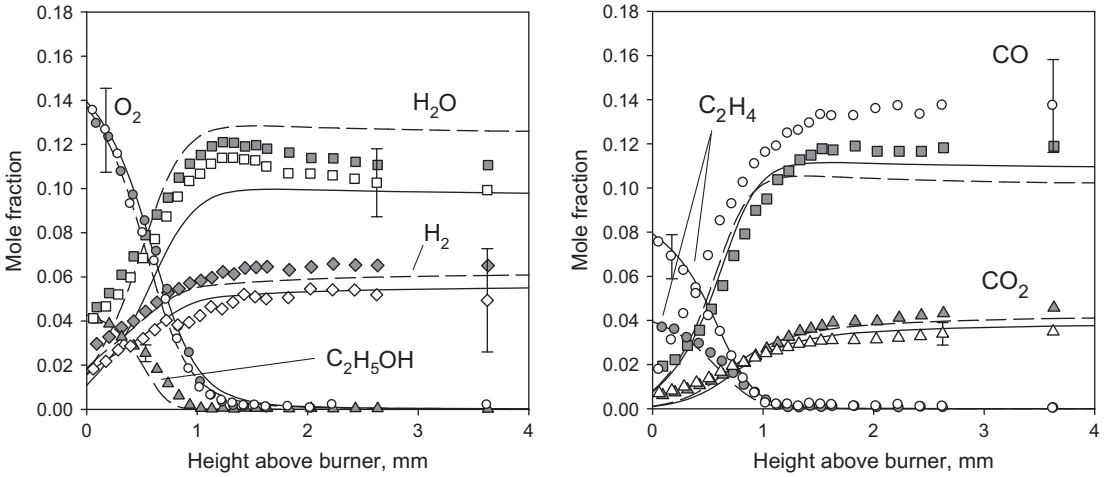

Fig. 2. Mole fractions profiles of reactants and major products in pure ethylene and ethylene/ethanol flames. Symbols: experiment, lines: modeling using mechanism 1. Open symbols and solid lines are for pure ethylene flame, filled symbols and dashed lines correspond to ethylene/ethanol flame.

material balance in the post-flame zone, carbon-containing products other than CO and CO_2 were not taken into account.

4.2. C_1–C_2 hydrocarbons and oxygenated species

Figure 3 shows mole fraction profiles of methane, acetylene, and acetaldehyde and combined mole fractions of formaldehyde and ethane in the ethylene and ethylene/ethanol flames. As can be seen, the maximum mole fraction of these species in the flames is about 0.1–0.8%.

From the results of the experiment and all three models one can see that mole fraction of methane in each flame has a maximum in the flame zone from 0.5 to 1.0 mm above the burner and a certain level in the post-flame zone. The experiment shows that in the flame with ethanol, the mole fraction of methane is slightly lower throughout the whole flame zone than that in the pure ethylene flame. However, all models predict that ethanol addition to the unburnt mixture results in an increase of methane mole fraction in a zone up to 1 mm above burner. This means that the mechanisms do not reproduce the effect of the addition of ethanol to the fresh mixture on the methane mole fraction in the flame. However, they

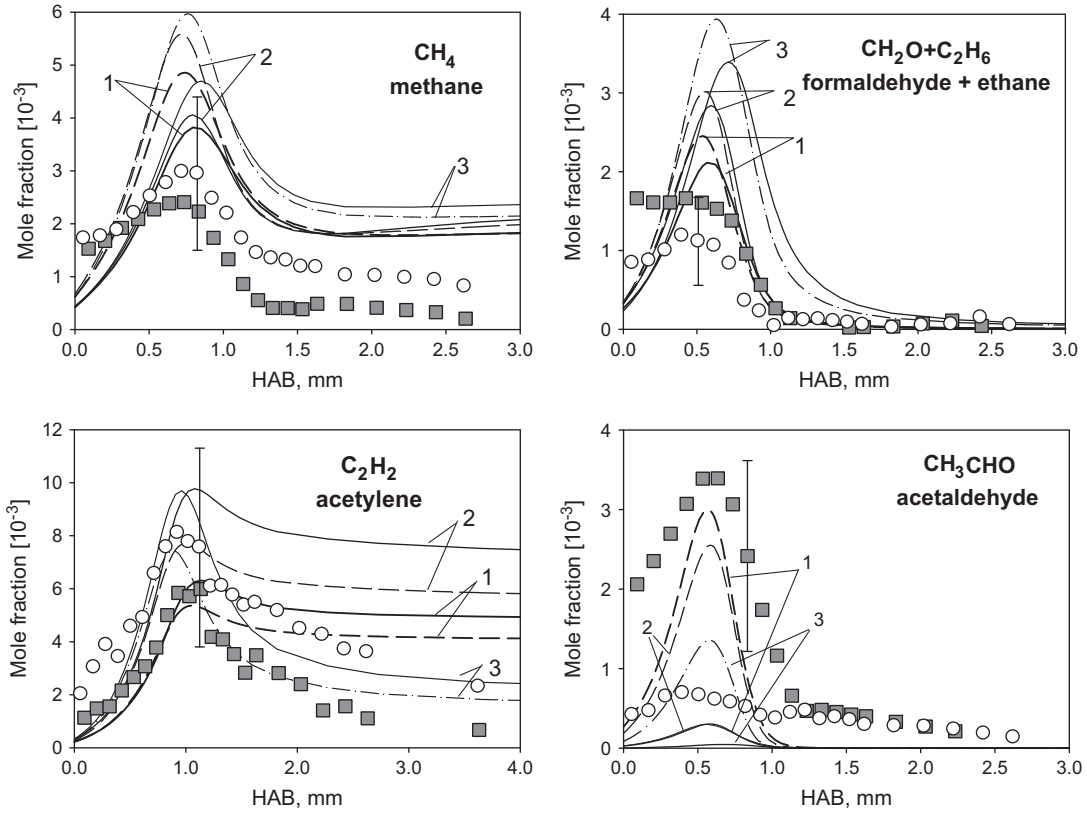

Fig. 3. Mole fraction profiles of C_1–C_2 hydrocarbon and oxygenated intermediates measured (symbols) in ethylene and ethylene/ethanol flames and calculated (lines) using three chemical kinetic mechanisms (numbered). Open symbols and solid lines correspond to pure ethylene flame; filled symbols and dashed lines are for ethylene/ethanol flame.

give good qualitative and quantitative predictions of the methane mole fraction profile in the pure ethylene flame.

The experimental data show that in the flame with ethanol, the maximum total mole fraction of formaldehyde and ethane is about 30% higher than that in the pure ethylene flame (upper right plot in Fig. 3). As can be seen from Fig. 3, an increase in the maximum total mole fraction of these species is also predicted by all the models considered. The models demonstrate that in the ethylene/ethanol flame, the maximum mole fraction of ethane is lower and the maximum mole fraction of formaldehyde is higher than in the pure ethylene flame. In particular, according to mechanism 1, in passing from the ethylene flame to ethylene/ethanol flame, the maximum mole fraction of ethane decreases from 6.1×10^{-4} to 5.1×10^{-4} and that of formaldehyde increases from 1.55×10^{-3} to 2×10^{-3}. This implies that an increase in the total mole fraction of these species in the ethylene/ethanol flame is due only to an increase in the mole fraction of formaldehyde.

In the flames studied, one of the major intermediate C_2 hydrocarbons is acetylene. According to our experimental data (bottom left plot in Fig. 3), its maximum mole fraction reaches 0.8% at about 1 mm from the burner surface in the pure ethylene flame. In the ethylene/ethanol flame, this maximum is also at 1 mm, but its magnitude is lower and reaches about 0.6%. The mole fraction of acetylene in both flames decreases monotonically with distance from the burner surface. All three mechanisms provide adequate predictions of experimental profiles of acetylene mole fraction at distances from the burner smaller than 1 mm. At a height of 1 mm or more, all mechanisms predict a monotonic decrease in acetylene mole fraction, as is observed in the experiment. However, in this zone, mechanisms 1 and 2 predict a slow consumption of acetylene: at 4 mm from the burner surface, its mole fraction in both flames is only about 20% lower than the maximum one. Only mechanism 3 (Konnov's model) gives a decrease in the acetylene mole fraction in this zone that is similar to that observed in the experiment. Specifically, the results of both the experiment and modeling with mechanism 3 indicate that in the ethylene flame at 3.5 mm from the burner, the mole fraction of acetylene is approximately four times lower than its maximum value.

The measurements and simulations with the three mechanisms show that the mole fraction of acetaldehyde (bottom right plot in Fig. 3) in the ethylene/ethanol flame is significantly higher than that in the pure ethylene flame. This was to be expected because acetaldehyde is one of the major products of ethanol oxidation. The experimental data presented for acetaldehyde are probably slightly overstated since propane (C_3H_8) can contribute to the signal intensity at $m/z = 44$. In addition, the modeling predicts its mole fraction to be an order of magnitude lower than the mole fraction of acetaldehyde. The occurrence of a signal in the zone of about 1.0–2.5 mm from the burner surface is probably due to a contribution from some other species.

Figure 4 presents mole fraction profiles of ketene and propene. In the ethylene/ethanol flame, the measured maximum total mole fraction of these species is lower than in the pure ethylene flame. Simulations using all three mechanisms also show a reduction in the maximum of the total mole fraction of these species in passing from the ethylene flame to the ethylene/ethanol flame. However, as can be seen from the figure, the mechanisms give different maximum total mole fractions of these species. In particular, in the pure ethylene flame, it is approximately 3.0×10^{-3}, 0.7×10^{-3}, and 1.5×10^{-3} for mechanisms 1, 2 and 3, respectively. Since the total mole fraction of these species is determined experimentally to within a factor 2, it is difficult to conclude which of the models is more appropriate for predicting the mole fraction. One can say that all the models provide a qualitatively adequate description of the effect of ethanol on the total mole fractions of these species.

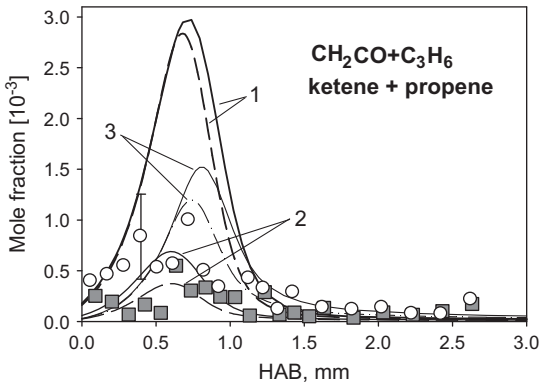

Fig. 4. Profiles of total mole fraction of ketene and propene measured (symbols) and calculated (lines) with three chemical kinetic mechanisms (numbered). Open symbols and solid lines correspond to pure ethylene flame; filled symbols and dashed lines are for ethylene/ethanol flame.

4.3. C_3–C_4 hydrocarbon intermediates

The mole fraction profiles of C_3H_4 and C_3H_3 (propargyl) are presented in Fig. 5, and those of diacetylene (C_4H_2) in Fig. 6. Propene, which was already discussed above, also belongs to this group of species (C_3–C_4 hydrocarbons).

The signal intensity at m/z corresponding to C_3H_4 is contributed mainly by allene and propyne; therefore, the experimental profiles for C_3H_4 presented in Fig. 5 are profiles of the total mole fraction of these species. The calculated profiles shown in this figure also correspond to the sum of the mole fractions of these species. All three models are seen to satisfactorily predict the mole fraction profiles of C_3H_4 in both flames. Similarly to the experimental data, they predict a reduction in the maximum mole fraction of C_3H_4 in the ethylene/ethanol flame.

As we have mentioned in the Experimental Procedure section, the profile of signal intensity at $m/z = 39$ corresponding to C_3H_3 was measured at a higher electron energy (12 eV) than those used by other authors (for example, 9.9 eV [24], 9 eV [40]). For this reason, we were not able to measure the signal intensity at $m/z = 39$ with an acceptable signal-to-noise ratio at energies lower than 12 eV. Since propargyl is a key species in rich flames as it takes part in the formation of soot precursors, we sought to measure its mole fraction. According to gas phase ion energetics data from the NIST Standard Reference Database [39], the signal intensity at $m/z = 39$ ($C_3H_3^+$) at an electron energy of 12 eV can also be contributed by C_3H_4 and C_4H_6 (1,3-butadiene). However, from data of [41], during photoionization at a photon energy of about 12 eV, the contribution to the $C_3H_3^+$ ion signal from $C_3H_4^+$ is less than 10%. If to assume that for electron ionization this contribution is also not significant (less than 10%), then the main contribution (except for propargyl) is from 1,3-butadiene ($m/z = 54$). We measured the intensity profile at $m/z = 54$ at an ionizing electrons' energy of 12 eV in the pure ethylene flame and performed direct calibration of our setup for 1,3-butadiene using a calibration mixture of 1,3-butadiene/argon. This procedure allowed us to determine that the mole fraction of 1,3-butadiene in the flame is not higher than 50 ppm. This amount of 1,3-butadiene contributes no more than 4% to the signal at $m/z = 39$ in the flame. Fig. S1 in Supplemental material (mmc4) shows an ionization efficiency curve for $m/z = 39$, which we measured in the ethylene flame at a height above burner of 0.8 mm (this corresponds to maximum of the signal at $m/z = 39$). This curve does not have any indications of possible contribution to the signal at $m/z = 39$ from fragmentation of other species. Therefore, under our experimental conditions, the major contribution to the signal at $m/z = 39$ is believed to be from propargyl.

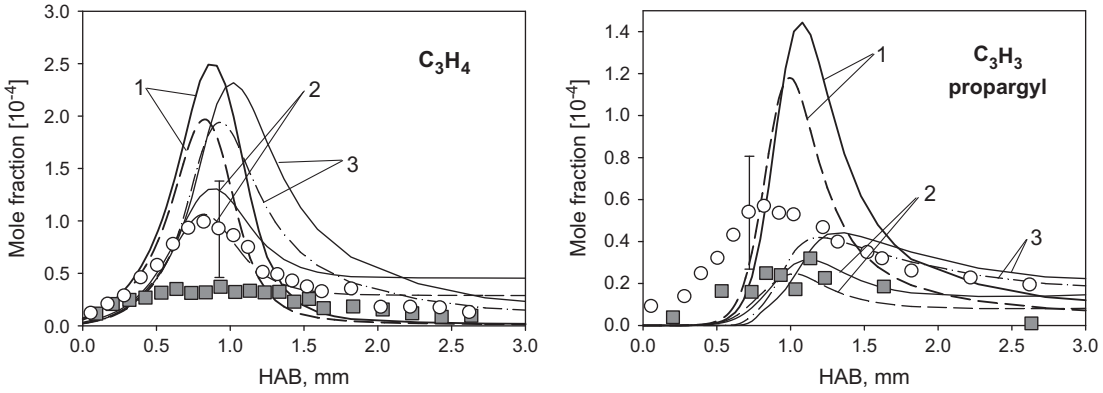

Fig. 5. Mole fraction profiles of C_3H_4 and propargyl radical measured (symbols) in ethylene and ethylene/ethanol flames and calculated (lines) using three chemical kinetic mechanisms (numbered). Open symbols and solid lines correspond to pure ethylene flame; filled symbols and dashed lines are for ethylene/ethanol flame.

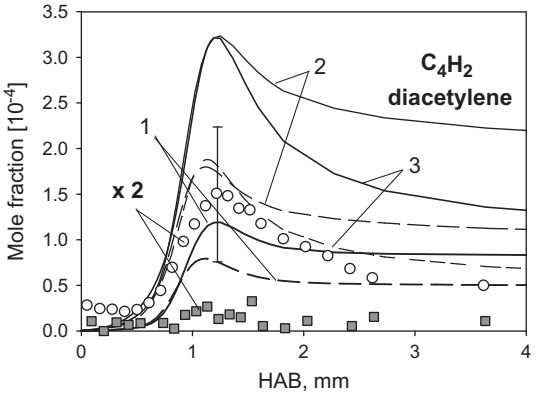

Fig. 6. Mole fraction profiles of diacetylene measured (symbols) and calculated (lines) using three mechanisms (numbered). Open symbols and solid lines correspond to pure ethylene flame; filled symbols and dashed lines are for ethylene/ethanol flame. Experimental mole fractions are multiplied by 2.

The measurements showed that the mole fraction of propargyl in both ethylene and ethylene/ethanol flames reached a maximum in a zone of 0.7–1.2 mm from the burner surface. In addition, the maximum mole fraction in the flame with ethanol was approximately half that in the pure ethylene flame. Although the simulation using three different mechanisms give different maximum mole fractions of propargyl in the flames, all the mechanisms predict that the maximum mole fraction of propargyl is lower (though only slightly) in the ethylene/ethanol flame than in the ethylene flame, as in the experiment. The experimental and numerical results are in agreement with our earlier experimental and numerical data for fuel-rich, premixed ethylene and ethylene/ethanol flames at low pressure [7], which also showed a reduction in the maximum mole fraction of propargyl when part of ethylene in the unburnt mixture was replaced with ethanol. Although we did not measure concentrations of soot and of aromatic species in the present work, the very fact that the addition of ethanol resulted in a reduction in the C_3H_3 mole fraction suggests a slowing of formation of soot precursors under the given conditions.

Similarly to our previous findings [7] for low-pressure conditions, at atmospheric pressure the experimental reduction of propargyl maximum mole fraction as ethanol is added to unburnt mixture is significantly higher than computational (about two times in experiment vs 1.2 or less times in modeling with different mechanisms). This indicates that the chemical kinetic models are unable to predict quantitatively the effect of ethanol addition to the flame of ethylene on C_3H_3 maximum mole fraction, while they are well in qualitative predicting. The results of a recent study by Frassoldati et al. [42] for propene and propene/ethanol fuel-rich premixed flames at 40 mbar also show that, when 50% of propene are replaced with ethanol, the experimental reduction of C_3H_3 mole fraction, which was measured using both EI-MBMS and MBMS with vacuum-ultraviolet photoionization [16], is about 2.2–2.5 times. However, the calculations performed in [42] using POLIMI mechanism [43] showed only ~1.4 times reduction of propargyl mole fraction. Therefore, the under-prediction of the reduction of C_3H_3 mole fraction due to ethanol addition is a common deficiency of all the models discussed above. In this context, the models have need of an improvement.

As in [7], in this work we analyzed the reaction pathways of propargyl formation in both flames in order to ascertain the reasons for the reduction in the maximum mole fraction of propargyl under the given conditions. According to all three mechanisms considered, the maximum of the rate of propargyl production and its mole fraction are in the range of heights above the burner from 1.0 to 1.3 mm. Below are the results of analysis of the reaction pathways of propargyl formation in this range, namely, at 1.1 mm.

Figure 7 shows the main pathways of propargyl formation in pure ethylene flame. Contributions, according to different mechanisms, to the total rate of production of each intermediate species through the pathways shown in Fig. 7 are listed in Table 2. Analysis of mechanism 1 for the ethylene flame showed that the main precursor of C_3H_3 is allene, which, reacting with H radicals ($aC_3H_4 + H \Longleftrightarrow C_3H_3 + H_2$) and OH radicals ($aC_3H_4 + OH \Longleftrightarrow C_3H_3 + H_2O$), provides 71.2% of the total rate of C_3H_3 production in this zone of the flame. A major contribution

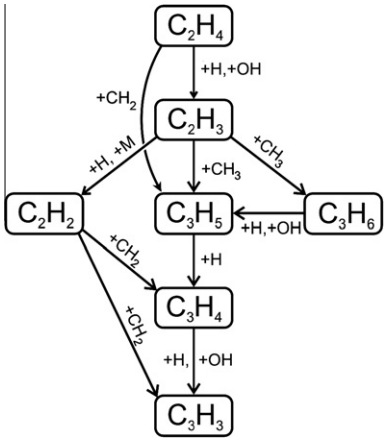

Fig. 7. The scheme of the main reaction pathways of propargyl formation in the pure ethylene flame.

Table 2
Contributions to the total rate of production of each intermediate species through the pathways shown in Fig. 7. C (consumption) means that the reactions providing the pathway proceed in reverse direction.

Major pathways (see Fig. 7)	Percentage of the total rate of production of the product		
	Mechanism 1	Mechanism 2	Mechanism 3
$aC_3H_4 \rightarrow C_3H_3$	71.2	11.6	14.5
$C_2H_2 \rightarrow C_3H_3$	25.7	60.8	21.8
$aC_3H_5 \rightarrow aC_3H_4$	90.8	53.5	38.0
$C_2H_3 \rightarrow aC_3H_5$	51.0	C	–
$C_2H_4 \rightarrow aC_3H_5$	9.2	48.5	–
$C_2H_4 \rightarrow C_2H_3$	93,0	89.0	92.2
$C_2H_3 \rightarrow C_3H_6$	18.0	16.4	81.0
$C_3H_6 \rightarrow aC_3H_5$	30.1	50.0	88.6
$C_2H_3 \rightarrow C_2H_2$	89.5	79.0	69.8
$C_2H_2 \rightarrow aC_3H_4$	C	C	29.4

(25.7%) to the rate of propargyl formation also comes from the reaction of acetylene with CH_2 ($C_2H_2 + CH_2 \Longleftrightarrow C_3H_3 + H$). Allene, in turn, is formed from the allyl radical through the reaction $aC_3H_5 + H \Longleftrightarrow aC_3H_4 + H_2$, which provides 90.8% of the total rate of C_3H_4 production. The allyl radical aC_3H_5 is formed from the vinyl radical C_2H_3 ($C_2H_3 + CH_3 \Longleftrightarrow aC_3H_5 + H$) or directly from ethylene ($CH_2 + C_2H_4 \Longleftrightarrow aC_3H_5 + H$), which, reacting with the H radical ($C_2H_4 + H \Longleftrightarrow C_2H_3 + H_2$) and OH radical ($C_2H_4 + OH \Longleftrightarrow C_2H_3 + H_2O$), provides 93% of the total rate of C_2H_3 production. Formation of C_3H_5 also occurs from C_2H_3 through propylene C_3H_6, but this pathway is not significant in the mechanism 1. Formation of acetylene also takes place in the reactions involving C_2H_3: the bimolecular decomposition $C_2H_3(+M) \Longleftrightarrow C_2H_2 + H(+M)$ and the reaction with the participation of a hydrogen atom $C_2H_3 + H \Longleftrightarrow C_2H_2 + H_2$. Together, these reactions give 89.5% of the total rate of C_2H_2 production. All these pathways are in many respects very similar to those at low pressure [7] (see Fig. S2 in Supplemental material (mmc4)). The only difference is that at atmospheric pressure acetylene contributes to C_3H_4 and C_3H_3 formation as described above, whereas these pathways are very weak at low pressure. Under low pressure conditions, the main reactions responsible for acetylene consumption are two reactions with atomic oxygen forming CH_2+CO and HCCO+H.

The reaction pathways described above also take place in mechanisms 2 and 3, and they differ only slightly. In particular, in mechanism 2, only 11.6% of C_3H_3 is formed from C_3H_4, and the main precursor of C_3H_3 is C_2H_2, whose reactions with CH_2 species in the ground and excited states provide 60.8% of the total rate of C_3H_3 production. The formation of C_2H_2 follows the same pathway: $C_2H_4 \rightarrow C_2H_3 \rightarrow C_2H_2$. The main feature that distinguishes mechanism 3 from mechanism 1 is that C_3H_5 is formed not directly from C_2H_3, but through propylene C_3H_6 ($C_2H_3 + CH_3 \Longleftrightarrow C_3H_6$), which reacts with the H radical ($C_3H_6 + H \Longleftrightarrow C_3H_5 + H_2$) and OH radical ($C_3H_6 + OH \Longleftrightarrow C_3H_5 + H_2O$) to yield C_3H_5.

The above analysis using all three mechanisms suggests that in the ethylene/ethanol flame, the pathways of propargyl formation are largely similar to those in the ethylene flame. C_3H_3 formation involves the same species starting from ethylene.

For ethanol, there are two main reaction pathways in the flame. According to mechanism 1, about 46% of the total consumption rate of ethanol are due to its decomposition to form C_2H_4 ($C_2H_5OH(+M) \Longleftrightarrow C_2H_4 + H_2O(+M)$) or C_2H_5 ($C_2H_5OH(+M) \Longleftrightarrow C_2H_5 + OH(+M)$), which is almost completely transformed to C_2H_4 ($C_2H_5(+M) \Longleftrightarrow C_2H_4 + H(+M)$). The remaining 54% of the total consumption rate of ethanol are due to the reactions producing oxygen-containing species, such as CH_2O and CH_2CO. These species react primarily with the formation of HCO and HCCO, which in turn yield CO and CO_2. Therefore, the part of ethanol that transforms through this pathway is not involved in the formation of propargyl and, apparently, the formation of soot precursors. In mechanisms 2 and 3, the ethanol consumption reactions producing ethylene contribute 44% and 39%, respectively, to the total consumption rate of ethanol. The remaining ethanol is involved in reactions leading to the formation of CH_2O and CH_2CO, which are finally oxidized to CO and CO_2.

Thus, from the results of modeling using the mechanisms considered, it follows that the reduction in the propargyl mole fraction in the atmospheric-pressure ethylene/ethanol flame compared to the pure ethylene flame is due to the existence of ethanol reaction pathway producing species that later do not yield C_3H_3. A similar conclusion for low-pressure conditions was made in our previous work [7]. The pressure has, therefore, no crucial effect on the pathways of propargyl formation and on the mechanism of C_3H_3 reduction due to ethanol addition to ethylene flame.

As can be seen from the experimental data in Fig. 6, the maximum mole fraction of diacetylene is about five times lower in the ethylene/ethanol flame than in the pure ethylene flame. All three chemical kinetic models predict a decrease in the diacetylene mole fraction over the entire flame zone when ethanol is added to the fresh combustible mixture. However, this decrease is not as significant as in the experiment and is a factor of 1.4–1.7 for different mechanisms. Furthermore, attention is drawn to the difference between the experimental and simulated ratios of the maximum mole fraction of diacetylene to its mole fraction in the post-flame zone (for definiteness, at 4 mm from the burner). In particular, for the ethylene flame, the experimental value of this ratio is about 3. As for modeling with mechanisms 1 and 2, this ratio is about 1.4, and according to simulation with mechanism 3, this ratio is closer to that derived from the experiment and is approximately 2.5. Thus, one can see that as in the case of acetylene, mechanisms 1 and 2 give a smaller decrease in the diacetylene level in the post-flame zone than those observed in the experiment and in simulation using mechanism 3. The indicated discrepancies for both acetylene and diacetylene motivated us to analyze mechanisms 1–3 in order to ascertain the reasons for the overestimation of the mole fractions of these species in the post-flame zone and to modify mechanisms 1 and 2 to resolve the discrepancies. The results obtained are discussed in the section below.

4.4. Analysis of the mechanisms and modification of mechanisms 1 and 2

To determine the reasons for the overestimation of the acetylene level in the post-flame zone by mechanisms 1 and 2, we calculated the sensitivity coefficients of C_2H_2 to all reactions and performed an analysis of the reaction pathways responsible for production and consumption of acetylene at different heights above the burner in the pure ethylene flame for all three mechanisms.

In the zone with the maximum production rate of acetylene (0.8–1.2 mm), the main reactions of its transformation and its production and consumption rates turned out to be similar for different mechanisms. However, as the post-flame zone is approached, there is a significant difference in the pathways of C_2H_2 consumption between the mechanisms. The calculations showed that in mechanism 3 (Konnov's mechanism), reaction R1 plays the greatest role in the post-flame zone:

$$C_2H_2 + OH \Longleftrightarrow CH_2CO + H \qquad (R1)$$

Its contribution to the total consumption rate of acetylene reaches 67.7% in the post-flame zone. In mechanisms 1 and 2, this reaction gives only 39.2% and 17.6% of the total consumption rate, respectively. That substantial difference in reaction rate could be attributed to the difference between the reaction rate constants used in these mechanisms. In mechanisms 1 and 2, the reaction rate constant is given by $k_{R1} = 2.18 \times 10^{-4} T^{4.5} \exp(1000/RT)$, the

units are cm, mole, cal, K. This expression was first proposed by Miller and Melius [44]. Woods and Haynes [45] measured concentrations of different hydrocarbons in rich ethylene/air flames at atmospheric pressure and compared their data with the results of flame structure modeling using the mechanism [44]. They encountered the same problem as we do: the kinetic mechanism they used overestimated the concentrations of C_2H_2 and CH_4 in the post-flame zone compared to their experimental data. Woods and Haynes [45] proposed several modifications for the kinetic mechanism that allowed them to achieve good agreement between experimental and numerical results. In particular, they proposed to replace the rate constant for R1 with the following expression: $k_{R1} = 1.1 \times 10^{13}$ exp $(-7170/RT)$. The very expression is used in Konnov's mechanism for reaction R1.

Reaction (R2) plays the most important role in C_2H_2 production along the entire flame zone:

$$C_2H_3(+M) \Longleftrightarrow C_2H_2 + H(+M) \quad (R2)$$

In all mechanisms, this reaction contributes about 70–80% to the overall acetylene production in the zone of acetylene accumulation. In the post-flame zone, this reaction has lower significance; nevertheless, its contribution is about 20–30%. Therefore, reaction R2 plays a key role in the acetylene accumulation process, but its rate constant is specified differently in different mechanisms. In Konnov's mechanism, it is given by $k_{R2} = 2.1 \times 10^{14}$ exp$(-39{,}740/RT)$ [46]. USC-II mechanism uses the expression $k_{R2} = 3.86 \times 10^8 T^{1.62}$ exp $(-37{,}048/RT)$ [47], and in Frenklach's mechanism, reaction R2 is defined in the reverse form with the rate constant $k_{-R2} = 5.6 \times 10^{12}$ exp $(-2400/RT)$ [48]. Our calculations showed that in the flame zone up to 1.2 mm from the burner, the sensitivity coefficient of C_2H_2 to reaction R2 is twice that in the post-flame zone, i.e., an increase in the rate constant of reaction R2 will result in an increase in the difference between the maximum and post-flame levels of C_2H_2.

We replaced the rate constants of reactions R1 and R2 in mechanisms 1 and 2 by the constants used in mechanism 3 and recalculated the structure of the flames. As an example, C_2H_2 mole fraction profiles simulated in pure ethylene flame using the modified mechanisms 1 and 2 are presented in Fig. 8. For comparison, this figure also shows the experimental C_2H_2 profile and those calculated with the original mechanisms 1–3. It is evident from this figure that the modification resulted in a considerable reduction in the acetylene level in the post-flame zone, and, therefore, the modified mechanisms provide a better fit to the measured C_2H_2 profile. For the ethylene/ethanol flame the modified mechanisms also give better prediction of the C_2H_2 mole fraction profile.

The concentration of diacetylene C_4H_2 depends strongly on the concentration of C_2H_2, because of the rapid interconversion between these species by reactions R3 and R4:

$$C_4H_2 + OH \Longleftrightarrow C_2H_2 + HCCO \quad (R3)$$
$$C_2H_2 + C_2H \Longleftrightarrow C_4H_2 + H \quad (R4)$$

Thus, the replacement of the rate constants of reactions R1 and R2 also resulted in better agreement between the numerical and experimental profiles of C_4H_2 mole fraction. As an example, this is shown in Fig. 9 for the pure ethylene flame.

However, the modification of mechanisms 1 and 2 described above led to a factor of two increase in the calculated CH_4 level in the post-flame zone. This is mostly due to an increase in the CH_2CO mole fraction resulting from an increase in the R1 reaction rate, and, hence, an increase in the production rate of methyl radicals through reaction R5:

$$CH_2CO + H \Longleftrightarrow CH_3 + CO \quad (R5)$$

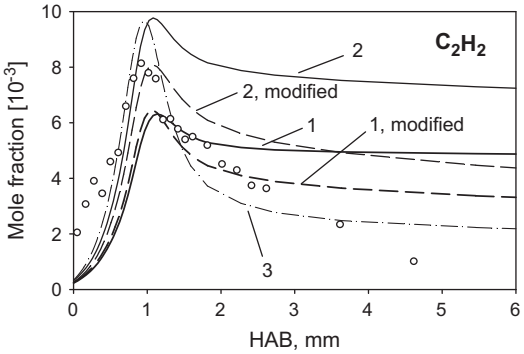

Fig. 8. Mole fraction profiles of acetylene in pure ethylene flame. Symbols correspond to experimental data, lines are modeling with different mechanisms (numbered) including modified ones.

A similar problem was encountered by Woods and Haynes [45]. To solve it, they proposed to add an additional channel of CH_2CO and CH_3 consumption (reaction R6) and to increase the rate constant of reaction R7.

$$CH_2CO + CH_3 \Longleftrightarrow C_2H_5 + CO \quad (R6)$$
$$CH_3 + OH \Longleftrightarrow CH_2OH + H \quad (R7)$$

Reaction (R7) accelerates consumption of methyl radicals, and, therefore, increasing its rate constant decreases the methane mole fraction in the post-flame zone. The rate constant of reaction R7 proposed in [45] for our temperature range (1600–1700 K) is about five times higher than that in mechanism 3, and more than an order of magnitude higher than those used in mechanisms 1 and 2. Following Woods and Haynes [45], we added reaction R6 to mechanisms 1 and 2 with the rate constant as proposed in [45] and changed the rate constant of reaction R7 to that recommended in [45]. The numerical calculations showed that this additional modification of mechanisms 1 and 2 adjusts the CH_4 mole fraction in the post-flame zone to the level predicted by the unmodified mechanisms 1 and 2. All the changes made in mechanisms 1 and 2 are indicated in Supplemental material (mmc4).

We checked that all the above-mentioned modifications in mechanisms 1 and 2 have only negligible influence on the mole fractions of the other species discussed in this paper. In addition, using the modified mechanism 1, we performed a simulation of the chemical structure of the low-pressure flames investigated in our previous work [7], and it was found that mechanism 1 with

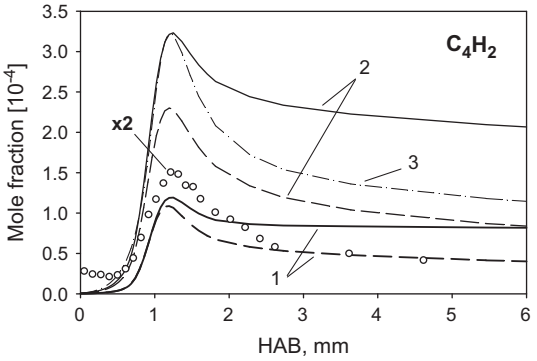

Fig. 9. Mole fraction profiles of diacetylene in ethylene flame. Symbols correspond to experimental data (multiplied by a factor of 2), lines are modeling with different mechanisms (numbered) including modified ones.

the modifications described above is as good as its original unmodified version in predicting experimental profiles under low-pressure conditions. The modifications of the mechanisms, suggested in this section, should be considered as a possible solution of a problem and as an invitation to those who develop the kinetic models to pay attention for the discrepancies (and their reasons) between models and experiment for acetylene and diacetylene mole fraction profiles.

5. Conclusions

Effect of ethanol on the species pool in a fuel-rich, premixed, burner-stabilized ethylene flame at atmospheric pressure was investigated. Mole fraction profiles of reactants, major products, and intermediate species (15 in total) in $C_2H_4/O_2/Ar$ and $C_2H_4/EtOH/O_2/Ar$ flames were measured using a molecular beam mass spectrometric setup and simulated numerically using three different chemical kinetic mechanisms available in the literature. This investigation showed that the main tendencies in ethanol effect on the species pool in premixed fuel-rich ethylene flame at atmospheric pressure remain in many ways the same as observed earlier for low pressure conditions [7]: the replacement of a half of ethylene with ethanol causes a reduction in mole fraction of C_xH_y hydrocarbons (C_2H_2, C_3H_4, C_3H_3), but results in increase of mole fraction of oxygenated hydrocarbons (formaldehyde, acetaldehyde). The comparison of the computed and measured mole fraction profiles of different species shows that the mechanisms qualitatively describe the structure of the flames under study and satisfactorily predict the general trend of the influence of ethanol addition on the mole fractions of major intermediate species in the ethylene flame.

Some discrepancies between the measurement data and simulation results obtained using the models based on the Frenklach [17,18] and USC II [36] mechanisms were observed for acetylene and diacetylene in the post-flame zone of the flames. Analysis of the reaction pathways in the mechanisms allowed us to identify the reactions responsible for the formation and consumption of the intermediates.

Modification of some reaction rates and reaction pathways in these mechanisms made it possible to improve their predictive capability with respect to mole fraction profiles of acetylene and diacetylene.

The experimental and modeling results indicate that the mole fraction of propargyl radicals, the main precursors of benzene and PAHs, is lower in the ethylene/ethanol flame than in the ethylene flame, indicating that ethanol contributes to the suppression of PAH formation. However, the mechanisms under-predict quantitatively the reduction of C_3H_3 mole fraction due to ethanol addition, indicating that they have need of a further improvement. Analysis of the main pathways of propargyl formation in the flame with and without ethanol has shown that the mechanism of propargyl reduction consists in the fact that when part of ethylene is replaced with ethanol in the unburnt mixture, the fraction of carbon forming propargyl decreases due to the existence of ethanol reaction pathways forming species that later do not yield C_3H_3. The mechanism of propargyl reduction due to ethanol addition to fresh mixture in atmospheric pressure conditions is, therefore, similar to that in low pressure conditions [7]. This fact together with that the general trends of ethanol effect on the species mole fractions in atmospheric and low pressure ethylene flames are very similar can indicate that the pressure has no noticeable effect on the mechanism of ethanol influence on the species pool in fuel-rich ethylene flames. Basing on this observation, we assume that this mechanism probably can work also at higher pressures, however, this is a topic of future research.

Acknowledgments

This work was supported by Siberian Branch of Russian Academy of Sciences under Lavrent'ev Grant #3 (2010–2011) for young scientists and Russian Foundation of Basic Research under Grant No. 10-03-00442-a.

Appendix A. Supplementary material

Supplementary data associated with this article can be found, in the online version, at doi:10.1016/j.combustflame.2011.12.022.

References

[1] K. Kohse-Höinghaus, P. Oßwald, T.A. Cool, T. Kasper, N. Hansen, F. Qi, C.K. Westbrook, P.R. Westmoreland, Angew. Chem. Int. Ed. 49 (2010) 3572–3597.
[2] B.Q. He, S.J. Shuai, J.-X. Wang, H. He, Atmos. Environ. 37 (2003) 4965–4971.
[3] T.S. Kasper, P. Oßwald, M. Kamphus, K. Kohse-Höinghaus, Combust. Flame 150 (2007) 220–231.
[4] N. Leplat, A. Seydi, J. Vandooren, Combust. Sci. Technol. 180 (2008) 519–532.
[5] N. Leplat, P. Dagaut, C. Togbe, J. Vandooren, Combust. Flame 158 (2011) 705–725.
[6] P. Saxena, F.A. Williams, Proc. Combust. Inst. 31 (2007) 1149–1156.
[7] O.P. Korobeinichev, S.A. Yakimov, D.A. Knyazkov, T.A. Bolshova, A.G. Shmakov, J. Yang, F. Qi, Proc. Combust. Inst. 33 (2011) 569–576.
[8] J. Wu, K.H. Song, T. Litzinger, S.-Y. Lee, R. Santoro, M. Linevsky, M. Colket, D. Liscinsky, Combust. Flame 144 (2006) 675–687.
[9] K. Kohse-Höinghaus, P. Oßwald, U. Struckmeier, T. Kasper, N. Hansen, C.A. Taatjes, J. Wang, T.A. Cool, S. Gon, P.R. Westmoreland, Proc. Combust. Inst. 31 (2007) 1119–1127.
[10] F. Inal, S.M. Senkan, Fuel 84 (2005) 495–503.
[11] J. Song, C. Yao, S. Liu, Z. Tian, J. Wang, Fuel 88 (2009) 2297–2302.
[12] C. Yao, X. Yang, R.R. Raine, C. Cheng, Z. Tian, Y. Li, Energy Fuels 23 (2009) 3543–3548.
[13] K.L. McNesby, A.W. Miziolek, T. Nguyen, F.C. Delucia, R.R. Skaggs, T.A. Litzinger, Combust. Flame 142 (2005) 413–427.
[14] C.S. McEnally, L.D. Pfefferle, Proc. Combust. Inst. 31 (2007) 603–610.
[15] B.A.V. Bennett, C.S. McEnally, L.D. Pfefferle, M.D. Smooke, M.B. Colket, Combust. Flame 156 (2009) 1289–1302.
[16] J. Wang, U. Struckmeier, B. Yang, T.A. Cool, P. Oßwald, K. Kohse-Höinghaus, T. Kasper, N. Hansen, P.R. Westmoreland, J. Phys. Chem. A 112 (39) (2008) 9255–9265.
[17] J. Appel, H. Bockhorn, M.Y. Frenklach, Combust. Flame 121 (2000) 122–136.
[18] H. Wang, M. Frenklach, Combust. Flame 110 (1997) 173–221.
[19] N.M. Marinov, Int. J. Chem. Kinet. 31 (1998) 183–220.
[20] O.P. Korobeinichev, S.B. Ilyin, V.V. Mokrushin, A.G. Shmakov, Combust. Sci. Technol. 116–117 (1996) 51–67.
[21] O.P. Korobeinichev, S.B. Ilyin, V.M. Shvartsberg, A.A. Chernov, Combust. Flame 118 (1999) 718–732.
[22] O.P. Korobeinichev, V.M. Shvartsberg, A.G. Shmakov, D.A. Knyazkov, I.V. Rybitskaya, Proc. Combust. Inst. 31 (2007) 2741–2748.
[23] A.G. Shmakov, O.P. Korobeinichev, I.V. Rybitskaya, A.A. Chernov, D.A. Knyazkov, T.A. Bolshova, A.A. Konnov, Combust. Flame 157 (2010) 556–565.
[24] A. Bhargava, P.R. Westmoreland, Combust. Flame 113 (1998) 333–347.
[25] T.A. Cool, K. Nakajima, K.A. Taatjes, A. McIlroy, P.R. Westmoreland, M.E. Law, A. Morel, Proc. Combust. Inst. 30 (2005) 1681–1688.
[26] J.D. Bittner, A Molecular Beam Mass Spectrometer Study of Fuel-rich and Sooting Benzene–Oxygen Flames, Ph.D. Thesis, Massachusetts Institute of Technology, 1981.
[27] E.L. Knuth, in: G.S. Springer, D.J. Patterson (Eds.), Engine Emissions: Pollutant Formation and Measurement, Plenum, New York, 1973, pp. 319–363.
[28] P.K. Sharma, E.L. Knuth, W.S. Young, J. Chem. Phys. 64 (1976) 4345–4351.
[29] Y.-K. Kim, K.K. Irikura, M.E. Rudd, M.A. Ali, P.M. Stone, J. Chang, J.S. Coursey, R.A. Dragoset, A.R. Kishore, K.J. Olsen, A.M. Sansonetti, G.G. Wiersma, D.S. Zucker, M.A. Zucker, <http://physics.nist.gov/PhysRefData/Ionization>.
[30] J.E. Hudson, M.L. Hamilton, C. Vallancey, P.W. Harland, Phys. Chem. Chem. Phys. 5 (2003) 3162–3168.
[31] W.L. Fitch, A.D. Sauter, Anal. Chem. 55 (1983) 832–835.
[32] W.E. Kaskan, Proc. Combust. Inst. 6 (1957) 134–141.
[33] C.R. Shaddix, Correcting thermocouple measurements for radiation loss: a critical review, in: Proceedings of the 33rd National Heat Transfer Conference, Paper HTD99-282, Albuquerque, New Mexico, 1999.
[34] O.P. Korobeinichev, A.G. Tereshchenko, I.D. Emel'yanov, A.L. Rudnitskii, S.Y. Fedorov, L.V. Kuibida, V.V. Lotov, Combust. Explo. Shock Waves 21 (1985) 524–530.
[35] K.H. Song, P. Nag, T.A. Litzinger, D.C. Haworth, Combust. Flame 135 (2003) 341–349.
[36] H. Wang, X. You, A.V. Joshi, S.G. Davis, A. Laskin, F. Egolfopoulos, C.K. Law, USC Mech Version II. High-temperature Combustion Reaction Model of H2/CO/C1-C4 Compounds, 2007. <http://ignis.usc.edu/USC_Mech_II.htm>.
[37] A.A. Konnov, Combust. Flame 156 (2009) 2093–2105.

[38] T. Turanyi, I.G. Zsely, C. Frouzakis, KINALC: A CHEMKIN Based Program for Kinetic Analysis, <http://www.chem.leeds.ac.uk/Combustion/Combustion.html>.
[39] P.J. Linstrom, W.G. Mallard (Eds.), NIST Chemistry WebBook, NIST Standard Reference Database Number 69, National Institute of Standards and Technology, Gaithersburg MD, 20899, <http://webbook.nist.gov>.
[40] P. Oßwald, H. Güldenberg, K. Kohse-Höinghaus, B. Yang, T. Yuan, F. Qi, Combust. Flame 158 (2011) 2–15.
[41] T.A. Cool, A. McIlroy, F. Qi, P.R. Westmoreland, L. Poisson, D.S. Peterka, M. Ahmed, Rev. Sci. Instrum. 76 (2005) 094102.
[42] A. Frassoldati, T. Faravelli, E. Ranzi, K. Kohse-Höinghaus, P.R. Westmoreland, Combust. Flame 158 (7) (2011) 1264–1276.
[43] A. Frassoldati, T. Faravelli, <http://creckmodeling.chem.polimi.it/kinetic.html>.
[44] J.A. Miller, C.F. Melius, Proc. Combust. Inst. 22 (1988) 1031–1039.
[45] I.T. Woods, B.S. Haynes, Proc. Combust. Inst. 25 (1994) 909–917.
[46] D.L. Baulch, C.J. Cobos, R.A. Cox, et al., J. Phys. Chem. Ref. Data 21 (1992) 411–429.
[47] V.D. Knyazev, I.R. Slagle, J. Phys. Chem. 100 (1996) 16899–16911.
[48] M. Frenklach, H. Wang, et al., <http://www.me.berkeley.edu/gri_mech/>.